A Triple-GEM Time Projection Chamber for Wide Field-of-View Hard X-ray Polarimetry: First Results

Davide Fiorina (D, ^{1,2} Elisabetta Baracchini (D, ^{1,2} Giorgio Dho (D, ³ Paolo Soffitta, ⁴ Samuele Torelli (D, ^{1,2} David J. G. Marques (D, ^{1,2} Enrico Costa, ⁴ Sergio Fabiani, ⁴ Fabio Muleri, ⁴ Giovanni Mazzitelli (D, ³ and Atul Prajapati (D^{5,2})

¹ Gran Sasso Science Institute, Viale F. Crispi, 7 67100 L'Aquila, Italy
 ² INFN Laboratori Nazionali del Gran Sasso, Via G. Acitelli, 22 67100 Assergi L'Aquila, Italy
 ³ INFN Laboratori Nazionali di Frascati, Via Enrico Fermi 54, 00044 Frascati (Roma), Italy
 ⁴ IAPS - INAF Istituto di Astrofisica e Planetologia Spaziali, Via del Fosso del Cavaliere 100, 00133 Roma, Italy
 ⁵ University of L'Aquila, Palazzo Camponeschi, Piazza Santa Margherita, 2, 67100 L'Aquila AQ

ABSTRACT

We report on the development of a large-volume, wide field-of-view time projection chamber (TPC) for X-ray polarimetry, featuring a triple-GEM amplification stage and optical readout. Originally developed within the CYGNO program for directional dark matter searches, the system employs a scientific CMOS (sCMOS) camera and a photomultiplier tube (PMT) to collect secondary scintillation light produced during charge amplification. A prototype with a cylindrical active volume (radius 3.7 cm, height 5 cm) was tested at the INAF-IAPS calibration facility (Rome, Tor Vergata) to assess sensitivity to low-energy electron directionality. We fully reconstruct electrons in the 10–60 keV range, obtain angular resolutions as good as 15°, and infer modulation factors up to 0.9. These first results demonstrate robust photoelectron tracking at tens of keV with strong modulation, indicating that photoelectric-effect polarimetry can be extended to higher energies. This capability is promising for rapid transients (GRBs, solar flares) and would broaden the astrophysical reach of X-ray polarimetry.

Keywords: Polarimeters (1277) — X-ray detectors (1815) — Astronomical instrumentation (799)

1. INTRODUCTION

X-ray polarimetry has recently emerged as a powerful diagnostic in high-energy astrophysics, adding polarization to the traditional observables (intensity, spectrum, timing) and enabling novel probes of magnetic-field geometry and radiation mechanisms in compact objects and shocks Costa et al. (2001); Weisskopf et al. (2010b). Advances in photoelectric polarimetry and the launch of NASA's Imaging X-ray Polarimetry Explorer (IXPE) Weisskopf et al. (2022) have made precise measurements routinely achievable, opening a new discovery space for extreme astrophysical environments. In the keV band, photoelectric polarimetry relies on reconstructing the emission angle of the photoelectron with respect to the incident photon direction. The ability to image and track low-energy electrons is also central to directional dark matter searches experiments such as CYGNO Amaro et al. (2022), which employs a gaseous TPC with triple-GEM amplification and optical readout to image low energy electron and nuclear recoils. Building on the proven performance of the CYGNO 50 L prototype for X-ray photoelectron imaging Amaro et al. (2023a), in this paper we investigate the extension of this experimental approach to hard X-ray polarimetry with a wide field of view.

1.1. Detector concept and experimental setup

The proposed experimental approach consists of a gas-filled drift region operated at an electric field of order 1 kV/cm. Ionization electrons produced by a particle interacting in the gas drift toward a GEM-based Sauli (1997)

Corresponding author: Davide Fiorina

davide. fiorina@gssi.it

amplification stage. In CF_4 -rich gas mixtures, ionization and avalanche processes generate excited fragments such as CF_3^* that de-excite via visible scintillation Fraga et al. (2003).

A scientific CMOS (sCMOS) camera focused directly on the last GEM foil, coupled to a fast photographic lens with a large numerical aperture, is employed to efficiently collect scintillation light and to image the track 2D projection with sub-millimeter spatial resolution Amaro et al. (2022, 2023a). A photomultiplier tube (PMT) records the time profile, enabling 3D track reconstruction and precise timing. While this last feature is already routinely used in CYGNO, it will be applied in the context of polarimetry after proper optimization in the near future, and for this reason, this paper focuses only on 2D imaging.

The prototype detector used in this work features a standard $10 \times 10 \text{ cm}^2$ thin triple-GEM amplification stage with 2 mm inter-GEM spacing operated with 2.5 kV/cm between them and the last electrode grounded. A cathode is positioned 5 cm above the first GEM, and a circular field cage of 7.4 cm diameter composed of silver wires encased in 3D printed plastic rings spaced about 1 cm ensures field uniformity in the drift region. The GEMs are powered by the HVGEM Corradi et al. (2007), a dedicated high voltage supply which works as an active high voltage (HV) divider. The TPC, typically operated in continuous gas flux mode, is enclosed in a 3D printed black plastic light-tight box that contains a gas-tight acrylic internal vessel. A thin window of highly transparent Mylar decouples the gas detector from the optical readout, which consists of a C14440-20UP ORCA-Fusion sCMOS camera placed at a distance of (20.5 ± 0.3) cm and focused through a Schneider Xenon lens on the last GEM plane. The camera possesses a squared silicon sensor of $1.498 \times 1.498 \text{ cm}^2$ area, segmented in 2304×2304 pixels. Each pixel features a Quantum Efficiency (Q.E.) of about 80% at 600 nm, and a readout noise of 0.7 electrons RMS. Within this scheme, the camera images an area of $\sim 11.3 \times 11.3 \text{ cm}^2$, resulting in an effective pixel size of $\sim 49 \times 49 \mu\text{m}^2$. Figures 1 and 2 show a schematic of the setup and actual picture of the detector, respectively, while Fig. 3 shows the relative Geant4 geometry simulated and used in the analysis discussed in Sec.2.1. For the measurements reported in this paper, not only the $He/CF_460/40$ gas mixture was employed representing the Dark Matter search standard in the CYGNO experiment context, but also alternative He/CF_4 ratios and Ar/CF_4 mixtures were explored as a better choice for the polarimetric approach.

A ⁹⁰Sr source is positioned between field-cage rings at the center of the drift gap, about 12 mm from the active volume, and a tungsten collimator (with 1 mm radius and 1 mm thickness) helps to focus the emitted electron directions. Energy calibration is performed with X-rays from ⁵⁵Fe (5.9 keV) and ¹⁰⁹Cd (22 keV and 80 keV) radioactive sources, and fitting the prototype response in terms of integrated pixel counts over the reconstructed track as a function of the absorbed nominal X-ray energy. The Orca Fusion sCMOS images are collected by a custom DAQ software based on MIDAS in free running mode and with 0.3 s exposure for ⁹⁰Sr and ⁵⁵Fe and 0.22 s for ¹⁰⁹Cd (due to the higher source activity).

2. LOW ENERGY ELECTRONS DETECTOR PERFORMANCES

The goal of the measurement campaign is to quantify the capability to reconstruct the initial direction of fully contained electron tracks. This requires deconvolving the measured angular distribution from the intrinsic angular spread of source electrons, evaluated with Geant4 Agostinelli et al. (2003). We thus derive the angular resolution as a function of electron energy. We then fold this resolution with a \cos^2 response to estimate the modulation factor μ for a fully polarized beam, and combine it with the intrinsic detection efficiency ϵ from simulations to obtain the figure of merit $\mu\sqrt{\epsilon}$, which directly enters the Minimum Detectable Polarization (MDP) Weisskopf et al. (2010a,b); Kislat et al. (2015).

2.1. Data analysis

Low-energy electrons emitted by the collimated ^{90}Sr source, primarily in a direction parallel to the GEM plane, were measured to evaluate the performance of the experimental approach in determining their initial direction. An example of a recorded track from an sCMOS image of a low-energy electron emitted by the ^{90}Sr source is displayed in Figure 4. The sCMOS images are analyzed, and the tracks are reconstructed using the Directional iDBSCAN algorithm developed by the CYGNO collaboration Baracchini et al. (2020); Amaro et al. (2023b). The algorithm groups pixel clusters that exceed a threshold using DBSCAN (Figure 5), taking directional information into account to merge clusters originating from the same track (Figure 6). A dedicated algorithm based on Principal Component Analysis and adapted from the one used by the IXPE collaboration Baldini et al. (2021) was optimized for the recorded sCMOS images to reconstruct the impact point and the direction of the measured tracks Torelli (2024). The steps of the algorithm are shown in Figure 8. After all the tracks were reconstructed and their directions estimated, selection

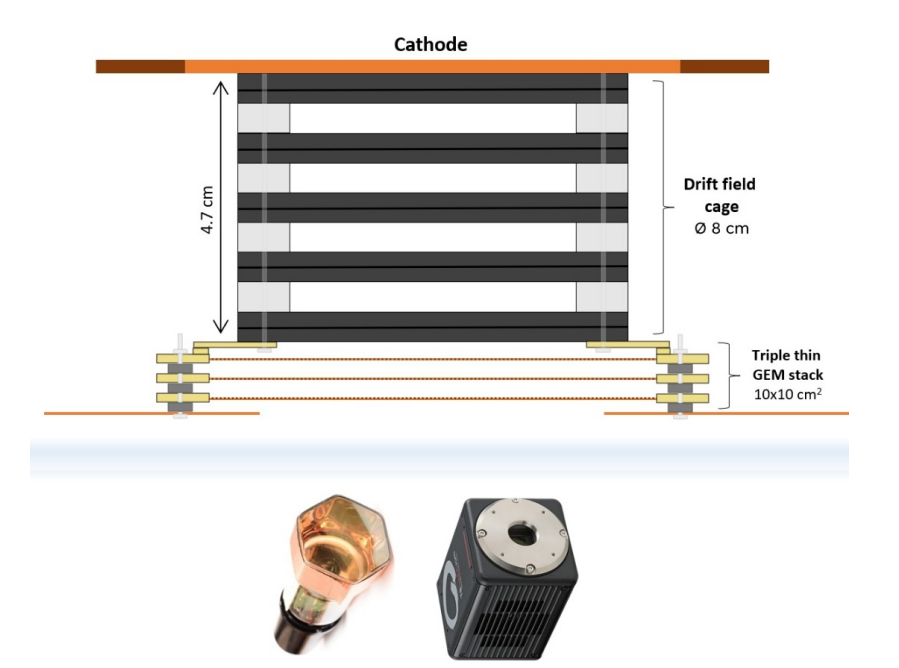


Figure 1. Schematic of the detector used in this work.

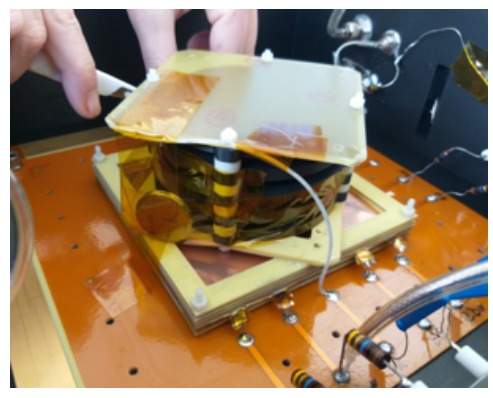


Figure 2. Photograph of the detector.



Figure 3. Geant4 simulation geometry for comparison with data.

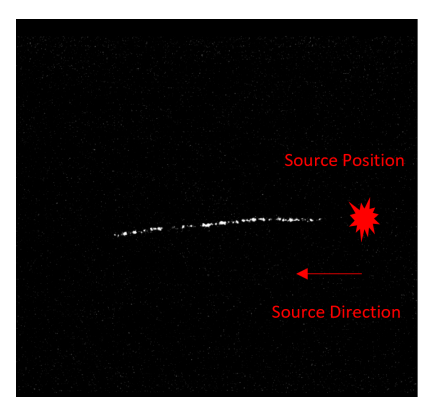


Figure 4. Contained electron track as seen by the camera. The source position and direction is highlighted.



Figure 5. First step on the reconstruction algorithm, clusters of pixels over the threshold are grouped.



Figure 6. Directional part of the reconstruction algorithm merges the clusters that come from the same track.

Figure 7. Reconstruction algorithm workflow.

cuts were applied to clean the sample for further analysis. Quality selection cuts retain events with interaction points (IP) within a radius of 5 mm around the source position (to suppress natural radioactive background contamination) and reject tracks with hits within 5 mm of the sensitive volume border (to ensure containment). Figure 9 displays the energy spectrum of the electron tracks resulting from this selection for the data acquired with the He/CF_4 60/40 gas mixture.

As previously discussed, a simulation of the intrinsic angular spread of the electrons from the source was performed to estimate the intrinsic electron tracks angular spread. Figure 3 shows a schematic of the simulation, where the sensitive cylindrical volume is modeled together with the field cage rings made of PMMA with an internal silver electrode. Electron track hits are recorded only within the sensitive volume, and the same selection cuts used in the data analysis for fully contained tracks are also applied to the simulated events. The initial direction of each electron track is determined by fitting a straight line to the projection of the first four hits on the GEM plane within the sensitive

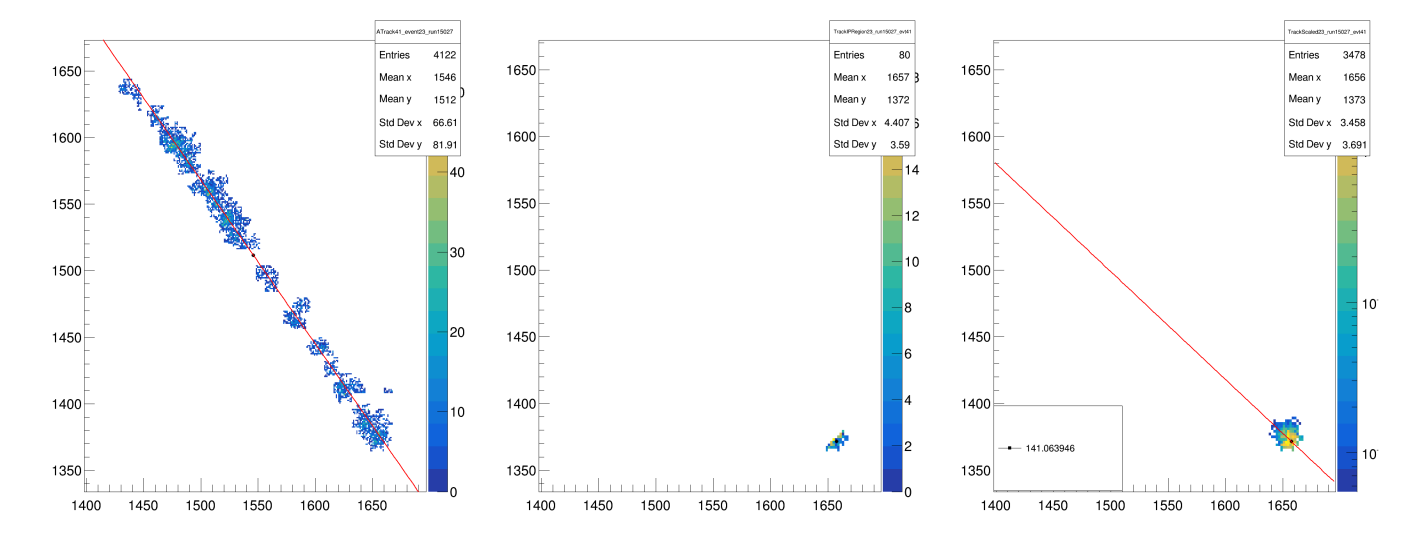


Figure 8. Directional algorithm on a fully contained track. Left: the original track with the barycenter and the principal axis. Center: the Interaction Point found by the algorithm. Right: selected and weighted points for direction computation with the estimated real direction.

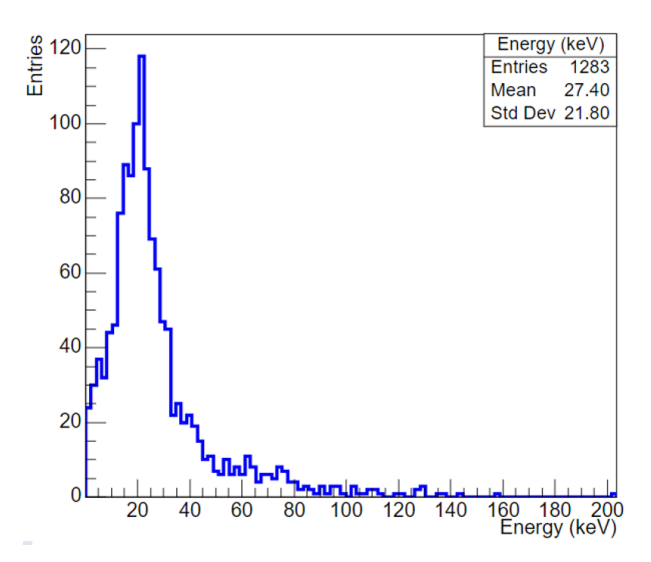


Figure 9. Calibrated energy spectrum of fully-contained tracks with correctly reconstructed IP for the data acquired with the He/CF_4 60/40 gas mixture.

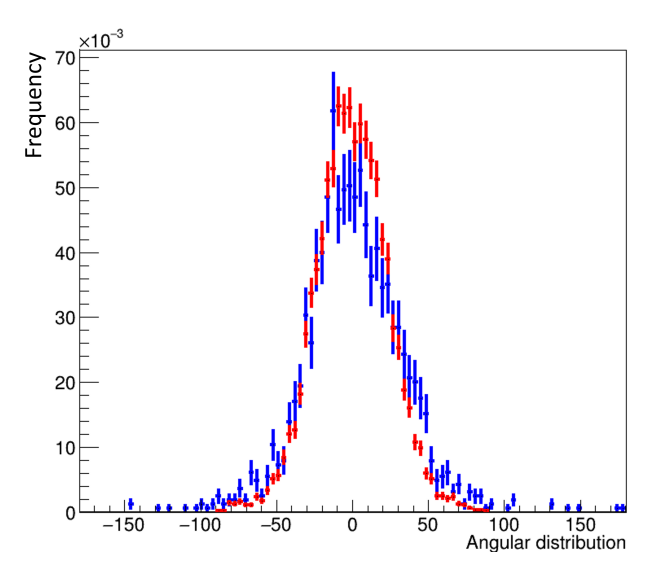


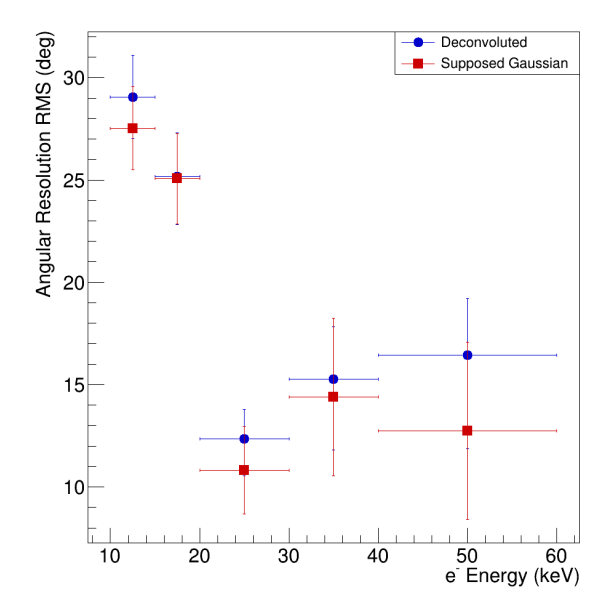
Figure 10. Intrinsic angular spread (RMS $\simeq 24^{\circ}$, red) from Geant4 vs. measured spread (RMS $\simeq 32^{\circ}$, blue) for the He/CF_4 60/40 gas mixture.

volume. The intrinsic spread obtained in this way, with an RMS of $23.6 \pm 0.2^{\circ}$, is shown in Figure 10, alongside the measured spread of $32.3 \pm 0.8^{\circ}$.

The measured angular distribution is then deconvolved from the intrinsic angular spread obtained from the GEANT4 simulation to extract the actual detector angular resolution. This deconvolution is performed using the Richardson–Lucy iterative method Richardson (1972); Lucy (1974). The RMS of the deconvolved distribution corresponds to the detector's angular resolution, which is reported in Figure 11 for different energy bins. Additionally, Figure 11 shows the resolution obtained from a simple quadratic subtraction of the RMS values:

$$RMS_{detector} = \sqrt{RMS_{measured}^2 - RMS_{intrinsic}^2},$$

which assumes that both distributions are perfectly Gaussian. The close agreement between the two approaches confirms the validity of the deconvolution procedure.



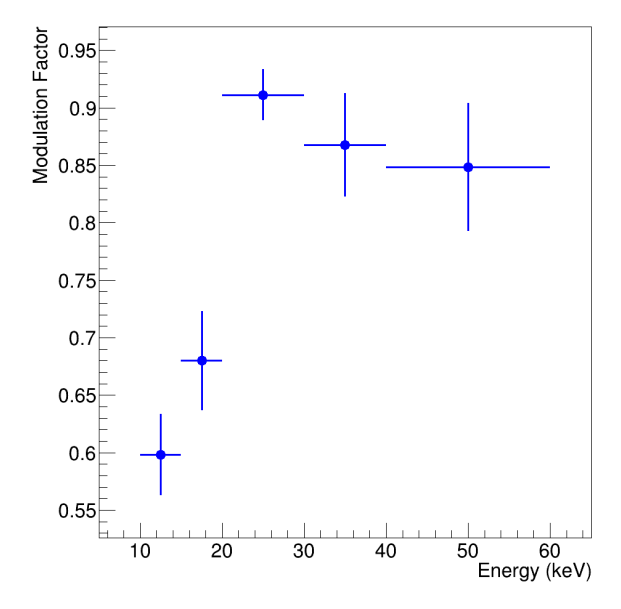


Figure 11. Measured angular resolution as a function of the calibrated electron energy. Blue: resolution obtained by deconvolution. Red: resolution obtained by quadratic subtraction of the measured and intrinsic spreads.

Figure 12. Expected modulation factor as a function of the X-ray energy for an optical readout polarimeter.

With the reasonable assumption that similar performance can be achieved for photoelectrons emitted from the absorption of polarized X-rays, the measured angular resolution can be treated as a Gaussian response applied to \cos^2 -modulated electrons. The expected distribution is expressed as:

$$(G * \cos^2)(x) = \frac{1}{2} (1 + e^{-2\sigma^2} \cos(2x)).$$

The modulation factor, μ , can then be calculated using the formula:

$$\mu = \frac{\frac{N^{\text{max}}}{100\%} - \frac{N^{\text{min}}}{100\%}}{\frac{N^{\text{max}}}{100\%} + \frac{N^{\text{min}}}{100\%}}$$

Figure 12 shows the results. These preliminary results indicate that a small TPC prototype, based on the CYGNO experimental approach with a cylindrical sensitive volume of 5 cm in height and 3.7 cm in radius, operating with an He/CF_4 (60/40) gas mixture, may achieve a modulation factor greater than 0.6 for X-rays above 10 keV and greater than 0.8 for X-rays above 20 keV.

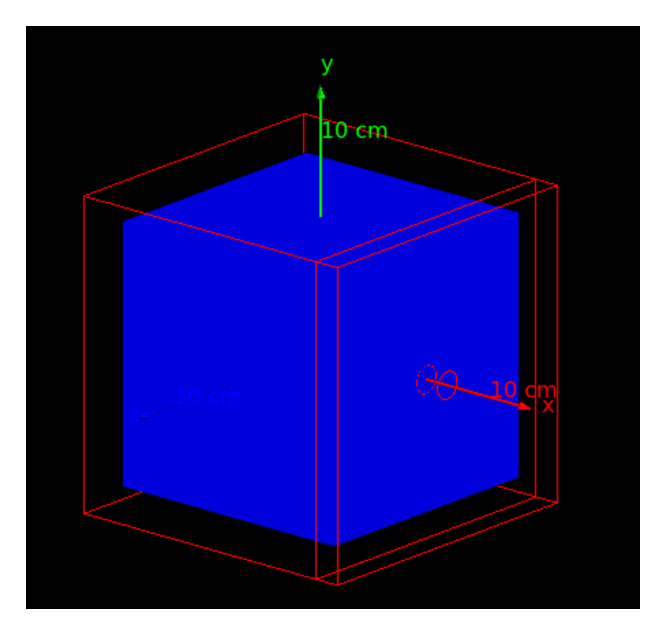
2.2. Detector polarimetric sensivity estimation

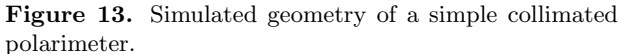
The Minimum Detectable Polarization (MDP) is a critical parameter for assessing the performance of a potential polarimeter. In the absence of background noise, the MDP can be expressed as Weisskopf et al. (2010a):

$$MDP = \frac{4.29}{\mu\sqrt{N}},$$

where N is the number of photons detected from the source. An effective polarimeter requires both a high modulation factor μ and high quantum efficiency ϵ , as these reduce the exposure time needed for a given source. Therefore, a useful figure of merit for characterizing a polarimeter is $\mu\sqrt{\epsilon}$.

We performed a Geant4 simulation to estimate the efficiency of a collimated polarimeter based on the results presented in Sec 2.1, with the goal of developing a compact instrument with a wide field of view. In the simulation, we modeled a gas cube with 10 cm sides, surrounded by 2 cm of aluminum shielding. The entrance window, placed at the center of one side of the shielding, has a diameter of 10.6 mm, corresponding to a potential maximum field of view





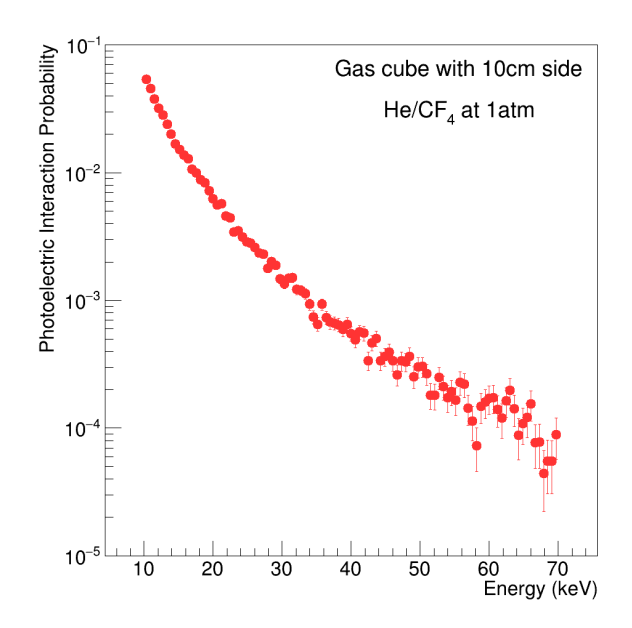


Figure 14. Simulated photoelectric efficiency.

of 27°. Although a realistic polarimeter would include a Micro Channel Plate (MCP) to select only photons incident perpendicularly on the entrance window, the MCP was omitted for simplicity in the simulation. Figure 13 illustrates the simulated geometry.

Photons with energies between 10 keV and 60 keV were simulated to enter through the entrance window. Secondary particles were tracked, and two conditions had to be satisfied for a photon to be counted as detected. First, the total deposited energy from the photon and its secondaries had to match the initial photon energy within 200 eV, to account for binding energies. Second, the initial photon had to interact only once in the sensitive volume, ensuring that it underwent a single photoelectric interaction.

Figure 14 shows the simulated efficiency for this configuration. The efficiency is relatively low for such a detector design, mainly due to the low density and atomic number of the CYGNO gas mixture, which was optimized for dark matter searches. To explore alternatives, we tested different gas mixtures by varying density and composition. Increasing the CF_4 content improves the efficiency approximately linearly, while replacing He with a higher-Z element such as Ar further enhances efficiency, owing to the Z^5 dependence of the photoelectric cross section.

The data collection and analysis procedure described above was then repeated for several gas mixtures at ambient pressure: He/CF_4 (40/60), Ar/CF_4 (60/40), and Ar/CF_4 (80/20). Figure 15 shows the angular resolutions obtained for the four gas mixtures. The angular resolution does not change significantly between mixtures, as it is primarily determined by the detector settings and analysis method, which are common to all. The impact of the gas mixture is more evident in Figure 16, where the higher efficiency of Ar-based mixtures improves the figure of merit by almost a factor of four compared to the CYGNO gas mixture. This translates into a substantial reduction in observation time, highlighting the advantage of Argon for enhancing detection performance.

3. CONCLUSION AND FUTURE PERSPECTIVES

We presented the first results from a triple-GEM TPC with optical readout, inspired by the CYGNO directional Dark Matter search approach, applied to hard X-ray polarimetry. Using collimated 90 Sr electrons, we demonstrated angular resolutions better than 30° above 10 keV and better than 20° for 20–60 keV electrons. Folding these resolutions with a \cos^2 response yields inferred modulation factors $\mu \gtrsim 0.6$ above 10 keV and $\mu \gtrsim 0.8$ for 20–60 keV. Further improvements in the proposed experimental approach performances are expected from optimization of gas pressure/density/composition (e.g., Ar-rich mixtures), as well as hardware and reconstruction improvements (3D timing via PMT, next-generation sCMOS, dedicated tracking). In addition to the results reported here, first measurements with fully polarized beams have already been performed at the INAF calibration facility in Rome Muleri et al. (2022),

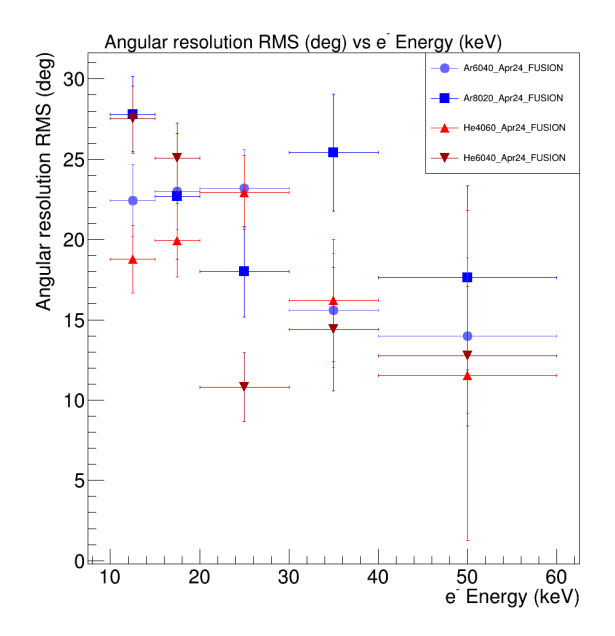


Figure 15. Measured angular resolutions for different gas mixtures.

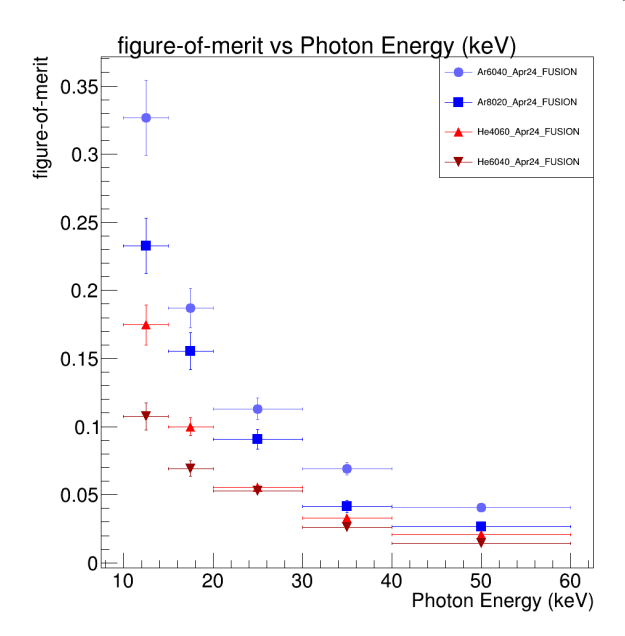


Figure 16. Expected figure of merit $\mu\sqrt{\epsilon}$ for the tested gas mixtures.

providing actual indications of the achievable realistic performance as a polarimeter, and a dedicated paper is in preparation.

These results strongly support the feasibility of a CYGNO-like optical TPC as a wide-FoV hard X-ray polarimeter. Such a detector could enable polarization measurements of rapid and unpredictable high-energy transients, such as gamma-ray bursts and solar flares Toma et al. (2009), magnetar giant flares Mereghetti (2008), tidal disruption events Komossa (2015), or multi-messenger sources including binary neutron star mergers Abbott et al. (2017). By opening sensitivity to such short-lived and rare phenomena, this technique would extend the reach of X-ray polarimetry into domains inaccessible to current narrow-field missions like IXPE, and provide unique synergies with future observatories across the electromagnetic and multi-messenger spectrum.

ACKNOWLEDGMENTS

This work is supported by the Italian Ministry of Education, University and Research (MIUR) through the PRIN project "HypeX: High Yield Polarimetry Experiment in X-rays" (Prot. 2020MZ884C_001).

REFERENCES

Abbott, B. P., Abbott, R., Abbott, T. D., et al. (LIGO Scientific Collaboration, & Collaboration), V. 2017,
Physical Review Letters, 119, 161101,
doi: 10.1103/PhysRevLett.119.161101

Agostinelli, S., et al. 2003, Nuclear Instruments and Methods in Physics Research Section A: Accelerators, Spectrometers, Detectors and Associated Equipment, 506, 250,

doi: https://doi.org/10.1016/S0168-9002(03)01368-8

Amaro, F., Antonietti, R., Baracchini, E., et al. 2023a, Eur. Phys. J. C, 83, 946,

doi: 10.1140/epjc/s10052-023-11988-9

Amaro, F. D., Antonietti, R., Baracchini, E., & otherss. 2023b, Measurement Science and Technology, 34, 125024, doi: 10.1088/1361-6501/acf402

Amaro, F. D., Baracchini, E., Benussi, L., et al. 2022, Instruments, $6, \, 6$

Baldini, L., et al. 2021, Astroparticle Physics, 133, 102628, doi: https://doi.org/10.1016/j.astropartphys.2021.102628

Baracchini, E., et al. 2020, Journal of Instrumentation, 15, T12003, doi: 10.1088/1748-0221/15/12/T12003

Corradi, G., Murtas, F., & Tagnani, D. 2007, Nuclear Instruments and Methods in Physics Research Section A: Accelerators, Spectrometers, Detectors and Associated Equipment, 572, 96,

doi: https://doi.org/10.1016/j.nima.2006.10.166

- Costa, E., Soffitta, P., Bellazzini, R., et al. 2001, Nature, 411, 662, doi: 10.1038/35079508
- Fraga, M., Fraga, F., Fetal, S., et al. 2003, Nuclear Instruments and Methods in Physics Research Section A: Accelerators, Spectrometers, Detectors and Associated Equipment, 504, 88,
 - doi: https://doi.org/10.1016/S0168-9002(03)00758-7
- Kislat, F., Beilicke, M., Guo, Q., & Krawczynski, H. 2015, Astroparticle Physics, 68, 45,
 - doi: 10.1016/j.astropartphys.2015.02.007
- Komossa, S. 2015, Journal of High Energy Astrophysics, 7, 148, doi: 10.1016/j.jheap.2015.04.006
- Lucy, L. B. 1974, The Astronomical Journal, 79, 745, doi: 10.1086/111605
- Mereghetti, S. 2008, Astronomy and Astrophysics Review, 15, 225, doi: 10.1007/s00159-008-0011-z
- Muleri, F., Piazzolla, R., Di Marco, A., et al. 2022, Nuclear Instruments and Methods in Physics Research A, doi: DOI_from_original_source
- Richardson, W. H. 1972, J. Opt. Soc. Am., 62, 55, doi: 10.1364/JOSA.62.000055

- Sauli, F. 1997, Nucl. Instrum. Meth. A, 386, 531, doi: 10.1016/S0168-9002(96)01172-2
- Toma, K., Sakamoto, T., Zhang, B., et al. 2009,Astrophysical Journal, 698, 1042,doi: 10.1088/0004-637X/698/2/1042
- Torelli, S. 2024, Feasibility of a directional solar neutrino measurement with the CYGNO/INITIUM experiment. https://arxiv.org/abs/2408.03760
- Weisskopf, M., et al. 2022, Journal of Astronomical Telescopes, Instruments, and Systems, 8, 026002, doi: 10.1117/1.JATIS.8.2.026002
- Weisskopf, M. C., Elsner, R. F., & O'Dell, S. L. 2010a, in Space Telescopes and Instrumentation 2010: Ultraviolet to Gamma Ray, ed. M. Arnaud, S. S. Murray, & T. Takahashi, Vol. 7732, International Society for Optics and Photonics (SPIE), 77320E, doi: 10.1117/12.857357
- Weisskopf, M. C., Elsner, R. F., & O'Dell, S. L. 2010b, in Proc. SPIE 7732, Space Telescopes and Instrumentation 2010: Ultraviolet to Gamma Ray, Vol. 7732, 77320E, doi: 10.1117/12.857357